The application of stereotomography to the Hussar 2D survey

Bernard Law and Daniel Trad

ABSTRACT

The results of applying stereotomography are presented. The effectiveness, limitations and the characteristics of stereotomography are demonstrated using synthetic data from a wedge model and the Marmousi model. The data preparation, the picking procedure and the quality of the Stereotomography solution is demonstrated using the vertical component of the Hussar 2D dataset and well logs.

INTRODUCTION

Stereotomography belongs to the family of slope tomography methods (Sword, 1987) . Slope tomography characterizes each reflection ray path with its two-way traveltimes and apparent slopes or ray parameters of the reflection event on the corresponding shot and receiver gathers (Figure 1). In a shot gather the apparent slope of a reflection event recorded at a geophone represents the ray parameter P_g of that geophone, and it determines the ray path between reflection point and the geophone. Similarly, in the geophone gather the apparent slope of the same reflection event represents the ray parameters P_s of the shot, and it determines the ray path between the reflection point and the shot. Therefore, it is necessary to evaluate both the shot gather and receiver gather of a reflection event in slope tomography to establish the unique shot and geophone ray pairs. Hence, the name stereotomography was used by Billette and Lambar$\acute{e}$ to emphasis the shot and receiver ray segment pair for each localized reflection event. Figure 1a shows traces around the shot location $\boldsymbol{S}$ and geophone location R at the two-way traveltime T_{sr}. If the velocity of media is known, the shot and receiver ray segments can be reconstructed with P_s, P_g and T_{sr} (Figure 1b). The ray parameters P_s and P_g can be picked by tracking the reflection events or by automatic picking using the semblance of the localized shot and receiver slant stacks.

The advantages of slope tomography over classical reflection tomography (Bishop et al., 1985; Chiu and Steward, 1987) include the additional data measurements of shot and receiver ray parameters and the elimination of the requirement to pick continuous reflection events on pre-stack data; hence, making automated picking easier. Sword (1987) developed the first slope tomography method, also called CDR (Rieber 1936; Riabinkin 1957) tomography. This method reconstructs the shot and receiver ray segments by shooting rays from shot and receiver at surface using the picked P_s , P_g and ending the ray tracing when the sum of the traveltime of the shot ray segment and receiver ray segment equals the two-way traveltime, T_{sr}. Velocity of the media V is estimated by minimizing the position errors X_{err} of the end points of the ray segments (Figure 2a). However, this method is sensitive to the picking errors and can be unstable because the accuracy of the forward modelling depends greatly on the picked P_s and P_g. Stereotomography (Billette et. al, 1998, 2003) remedied this instability using the generalized formulation of the slope tomography method. The forward modelling of stereotomography involves ray tracing from a scatter point X toward the S and R at the surface, and is independent of P_s , P_g and T_{sr}. Therefore, it is independent of picked data and remedies the instability of the original slope tomography method. However, besides the media velocity this approach also requires the estimations of the scatter position and the ray path geometry parameters for each local reflection event. This results in a more complex multi-parameter inversion problem (Figure 2b). The model space of stereotomography includes V, X, the shooting angle θ_s and traveltime T_s for the shot ray segment, and the shooting angle θ_g and traveltime T_r for the receiver ray segment. The data space includes S, R, P_s, P_g and T_{sr} . Picking of reflection arrival times and slopes are flexible in stereotomography, and can be based on maximum semblance of the shot and geophone slant stacks. However, for noisy data and in areas of complex structure, picking can still be a challenge. We will validate the accuracy of the stereotomography method using synthetic data created with a wedge model and the Marmousi model. We will also apply the stereotomography method to a 2D land data set acquired in the Hussar area of Alberta to demonstrate the data preparation, the picking procedure and the quality of the Stereotomography solution.

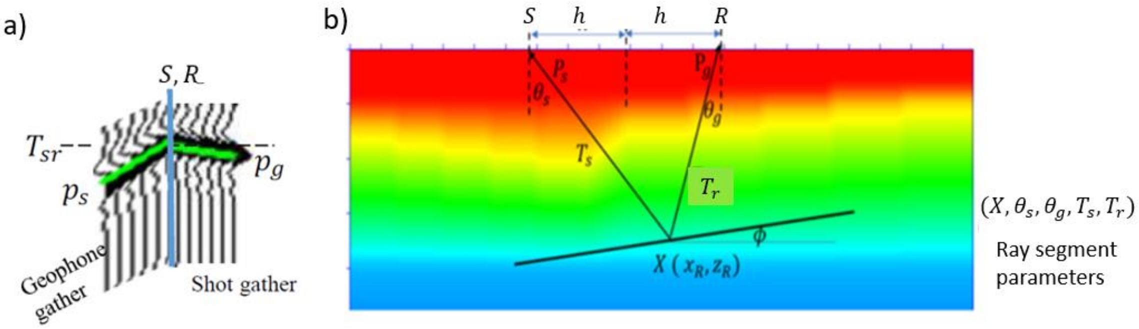

Figure 1 (a) Relationship between $T_{sr} P_s, P_g$ of a localized coherent event. (b) The event is characterized by the traveltime T_{sr} and the ray parameters p_s and p_g and is associated with a ray segment pair in the velocity model. Reflector dip ϕ and ray segment parameters including the scatter point location **X**, ray shooting angles θ_s and θ_g can be estimated from the half-offset *h*, the ray parameters, and two-way traveltime T_{sr}.

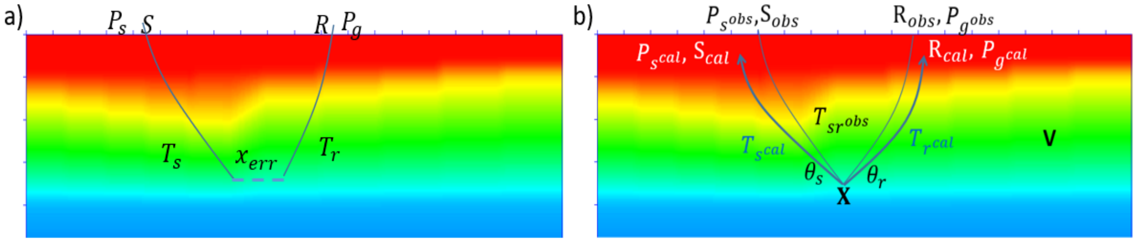

Figure 2 (a) CDR tomography shoots ray from surface using picked ray parameters P_s, P_g and estimates the velocity by minimizing the position error Xerr of the ray segment end points. (b) Stereotomography shoots rays from an estimated scatter point X to the shot and receiver, and estimates the velocity **V** and ray segment parameter **X**, θ_s , θ_g , T_s *and* T_r by minimizing the misfits of the data space parameters.

THEORY

Forward and inverse problem

In classical reflection tomography, the forward modelling of the traveltime tomography can be represented by:

$$t_{raypath} = \int_{raypath} s(x,z)dl, \qquad (1)$$

where the measured traveltime t is the integral of slowness $s(x,z)$ along the ray path.

If the line integral equation 1 defines a linear system, it can be represented in matrix form as:

$$\mathbf{d} = \mathbf{L}\ \mathbf{m}\ , \qquad (2)$$

where **d** is the travel time of a raypath, **m** is the slowness model, **L** is a matrix that contains the physical relationship between the measurements $\mathbf{t}$ and the model parameter $\mathbf{s}$. **L** is called the Kernel, Jacobian, Fréchet derivative or sensitivity matrix. For the line integral equation 1, **L** is of the dimension of number of data points by number of velocity cells. Each row of **L** contains the ray path segment length for each cell that a ray path has traversed to create a traveltime measurement.

The cost function or misfit function for equation 2 is:

$$J(m) = \parallel \mathrm{d} - \mathbf{L}\ \mathrm{m} \parallel^2 \qquad (3)$$

The linear least-squares solution of equation (3) is

$$\mathbf{m} = (\mathbf{L^T L}\ )^{-1}\mathbf{L}^T\mathbf{d}\,. \qquad (4)$$

Since ray path is a function of the slowness and line integral equation represent a non-linear system, equation 2 becomes:

$$\mathbf{d} = \mathbf{L}(\mathbf{m}), \qquad (5)$$

and the cost function for equation 4 is:

$$J(m) = \parallel \mathbf{d}\ - \mathbf{L}\ (\mathbf{m})\ \parallel^2. \qquad (6)$$

Because of the non-linearity of equation 5 and 6, the slowness model cannot be obtained directly using equation 4. However, the traveltime **d** is picked from the data; it is invariant or model independent. We can exactly calculate the cost function in equation 6; Therefore, the non-linear problem of classical reflection tomography can be linearized by iteratively solving:

$$\mathbf{\Delta d} = \mathbf{L}\ \mathbf{\Delta m}, \qquad (7)$$

where $\mathbf{\Delta m}$ is the model update vector between iterations, **L** is the Frechét derivative matrix $\partial L(m)/\partial m$, the partial derivatives of the modelled response with respect to the model parameters and $\mathbf{\Delta d}$ is the differences between the modelled traveltime and the observed traveltime.

Stereotomography

Unlike classical traveltime tomography that has only traveltime in the data space and slowness in the model space, stereotomography is a multiparameter problem (Figure 2b). It is necessary to include the data covariance $\mathbf{C_d}$ in the cost function:

$$J(m) = \left(\mathbf{d} - \mathbf{L}(\mathbf{m})\right)^{\mathbf{T}} \mathbf{C_d^{-1}} \left(\mathbf{d} - \mathbf{L}(\mathbf{m})\right) \quad . \qquad (8)$$

When the data covariance are uncorrelated, $\mathbf{C_d}$ **i**s a diagonal matrix with the diagonal elements being the square of the standard derivation $\boldsymbol{\sigma}$ of the data, and $\mathbf{C_d^{-1}}$ is also a diagonal matrix with the diagonal element being $1/\boldsymbol{\sigma}^{\mathbf{2}}$. Therefore $\mathbf{C_d}$ can be chosen according to the standard deviation of the data measurements. It is important to choose the appropriate unit for the data covariance, so that the data misfit of different data types is scaled accordingly. The data space of stereotomography includes S, R, T_{sr}, P_s and P_g. Data misfit Δd_i for each data point in equation 7 is:

$$\Delta d_i = ((S_{obs} - S_{cal})C_{d_S} \ , (R_{obs} - R_{cal})C_{d_R} \, , \left(T_{sr_{obs}} - T_{sr_{cal}}\right)C_{d_{Tsr}} \, , \\ \left(P_{s_{obs}} - P_{s_{pred}}\right) C_{d_{P_s}} \, , \left(P_{g_{obs}} - P_{g_{pred}}\right) C_{d_{P_g}}). \qquad (9)$$

The model space includes V, X_c , θ_s , T_s , θ_g and T_g . For each data point, the Fréchet derivative L_i in equation 7 is the combination of the derivatives of data space element with respect to the model space element:

$$L_i = \frac{\boldsymbol{\partial}(\mathbf{S},\mathbf{R},\mathbf{T_{sr}},\boldsymbol{P_s},\boldsymbol{P_g})}{\boldsymbol{\partial}(\mathbf{X_c},\boldsymbol{\theta_s},\boldsymbol{\theta_g},\boldsymbol{T_s},\boldsymbol{T_g},\boldsymbol{V_{1,m}})} \, . \qquad (10)$$

Each element of the Fréchet derivative L_i can be computed during paraxial raytracing (Cervený et al, 1977). With the data misfit Δd_i and the Fréchet derivative L_i for each data point established, model update $\mathbf{\Delta m}$ can be computed iteratively by solving equation 7 using conjugate-gradient method.

SYNTHETIC DATA EXAMPLE

To validate the accuracy of the stereotomography method, we create synthetic data sets using a wedge model and the Marmousi model. The wedge model (Figure 3a) consists of four constant velocity layers with the second layer thins out with increasing surface location. 200 shot gathers (Figure 3b) were created using finite-difference modelling with absorbing sponge boundaries. We picked a rough moveout velocity function (Figure 3c) at the middle of model and created a near-trace stack (Figure 3d) using traces with offset less than 1000 m. Reflection boundaries were picked on the near offset stacks and were used to track the reflection arrival times automatically on the moveout corrected CDP gathers (Figure 3e). Moveout correction was then removed from the picked reflection arrival times. Figure 3f shows a shot gather with picked reflection arrivals displayed in blue.

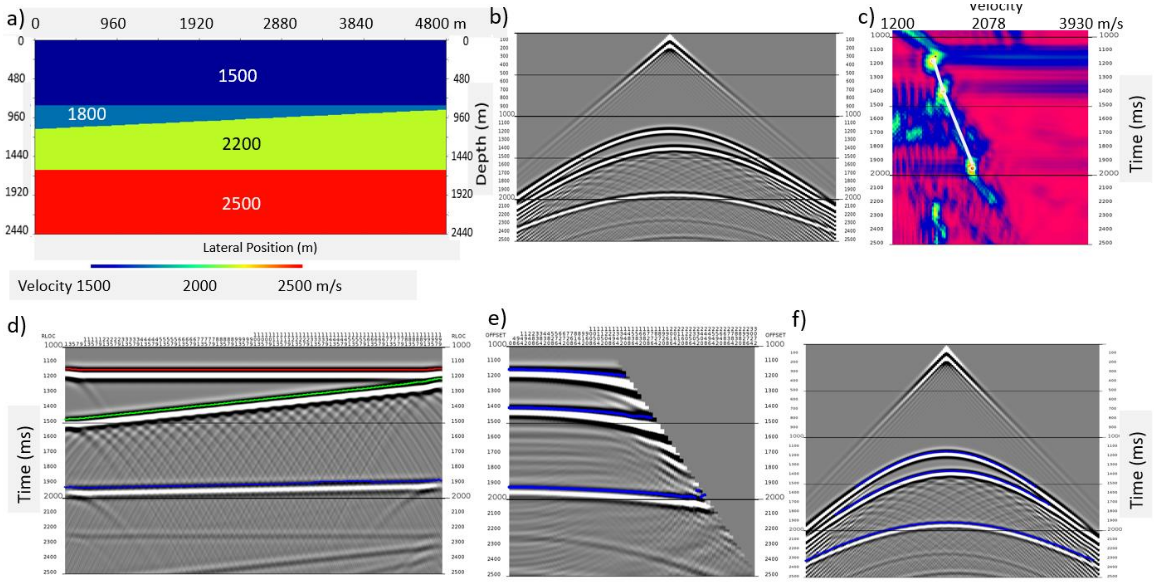

Figure 3 (a) Wedge model. (b) Finite difference shot gather. (c) Moveout velocity scans. (d) Near trace stack. (e) A moveout corrected CDP gather with refraction arrival times picked by correlation with the near-trace stack. (f) Shot gather with reflection arrival times.

We use the reflection arrival times to compute the shot and geophone ray parameters for stereotomography inversion. Figure 4a shows a shot gather with the two-way times and geophone slope picks. Figure 4b shows the quality control panels for each analysis location. Figure 4c shows the initial estimates of the scatter positions for all the stereotomography picks using straight ray and homogeneous media assumptions. The green lines in Figure 4c mark the dip bars computed from the 3 stereotomography picks.

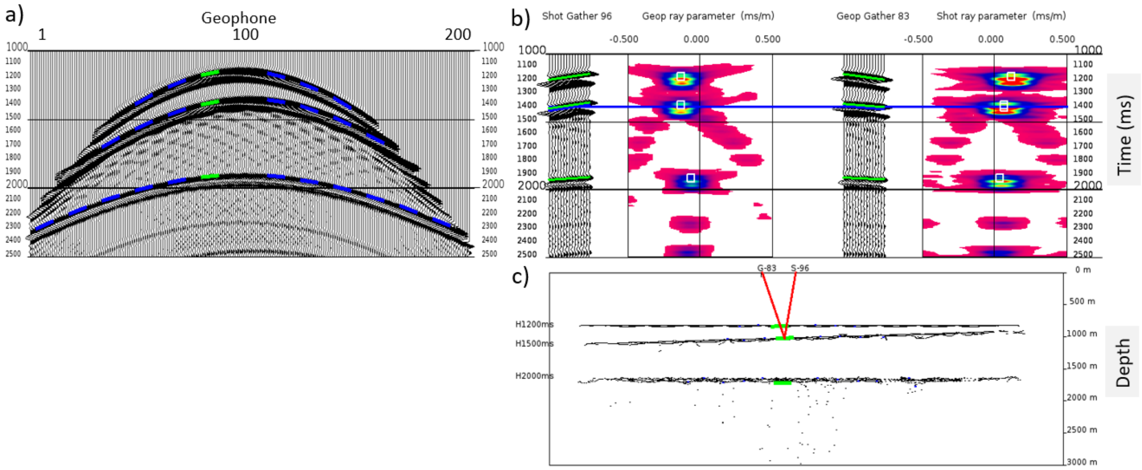

Figure 4 (a) A shot gather with two-way traveltime and geophone ray parameter picks. Green lines mark the picks for the active analysis location. (b) Quality control panels for an analysis location, (c) Initial estimates of the scatter positions. Green lines represent dip bars computed from stereotomography picks at the active analysis location.

We use the stereotomography picks to estimate the velocity V and ray segment parameters X, θ_s, T_s, θ_g and T_g. Figure 5a shows the final velocity solution with the velocity values at 6 locations displayed in white. Velocity values of the true model are displayed in black. Figure 5b shows the estimated scatter positions. Velocity solution from stereotomography does not capture the blocky characteristics of the wedge model, but it resembles velocity gradients centred around the true velocity values. The scatter positions match the velocity boundaries of the wedge model; hence, it is possible to develop a hybrid method that uses the scatter positions to establish the layer boundaries and modify the stereotomography algorithm to estimate a layered based velocity model. We estimate the velocity boundaries by linear fitting the computed scatter positions. The average velocity is computed by averaging stereotomography solution between layer boundaries (Figure 5c). Figure 5d displays the true velocity model with linear fitted scatter for comparison.

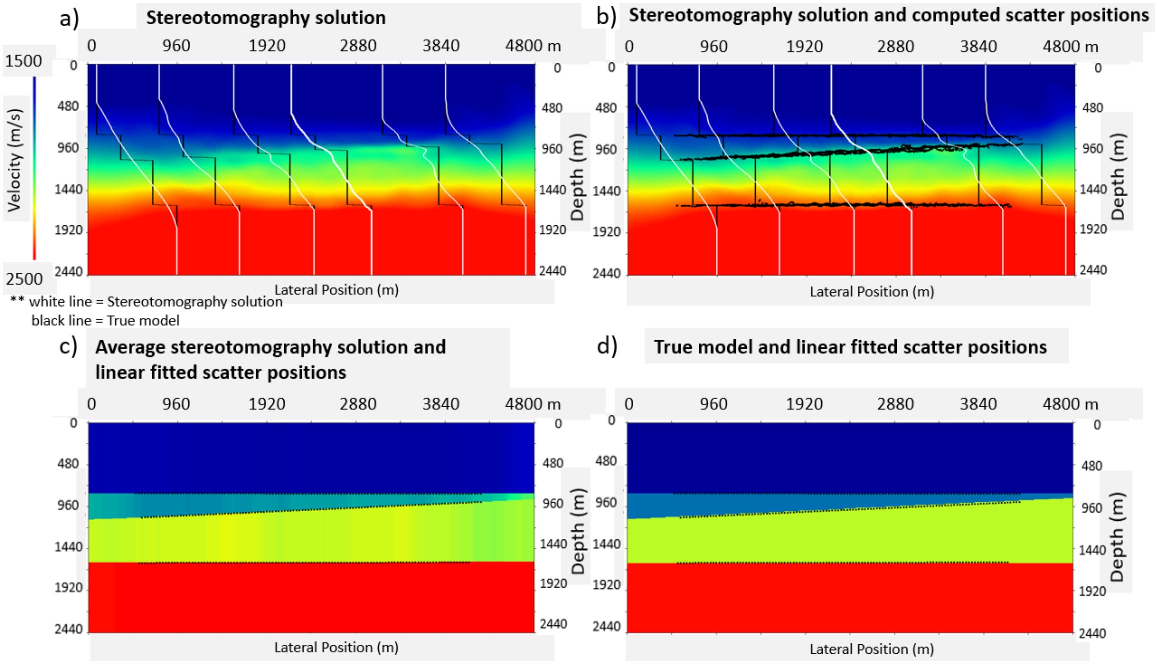

Figure 5 (a) Stereotomography solution of the wedge model synthetic dataset. Velocity values at 6 locations are displayed in white for the stereotomography solution and in black for the true model. (b) Scatter positions displayed as black dots. (c) Velocity layer boundaris are computed by linear fitting the computed scatter positions and displayed as black dots. Stereotomography solution is averaged between computed layer boundaries. (d) Linear fitted scatters positions displayed as block dots on the true velocity model.

We also use the Marmousi model (Figure 6a) to create 261 synthetic shot records with 96 traces per shot (Figure 6b). Both the shot spacing and geophone spacing are 25m. Because of the complex structures of the model and reflection signal, it is necessary to pick the reflection arrival times, shot and geophone ray parameters using semblance of the shot and geophone slant stacks. Figure 7a shows the picked reflection events on shot 248. Figure 7b shows the picked events and semblance at shot location 248 and geophone location 170. Figure 7c shows the initial estimates of the scatter positions for all the stereotomography picks using straight ray and homogeneous media assumptions. We use a constant velocity gradient as the starting model for stereotomography inversion. Figure 8a shows the final velocity solution, and figure 8b overlays the final scatter positions on the velocity solution. Comparing the stereotomography solution to the true model in figure 6a, the velocity solution captures the long wavelength trend of the true model up to about 2Km, and the scatter positions match the velocity boundaries in the true model. Figure 8c displays the velocity values from the stereotomography solution in white, and from the true model in black at 6 locations. This further confirms that the stereotomography solution does captures the long wavelength trend of the true model.

To evaluate the effectiveness of the stereotomography solution as a starting model for high resolution inversion method such as FWI, we perform FWI on the Marmousi data set using starting model from a constant vertical velocity gradient (Figure 9a) and from the stereotomography solution (Figure 9c). Figure 9b and 9d compare the FWI solution from the two starting models. FWI solution using the constant vertical velocity gradient as the starting model only captures some of high frequency velocity changes in the true model. FWI solution using the stereotomography solution as the starting model recovers most of the velocity features up to about 2Km. Details below 2Km are missing in the FWI solution. Potential improvement can possibly be using higher order finite-difference propagation in FWI and using the higher resolution multi-grid FWI approach proposed by Trad 2020, in which the high frequency field data will be shaped to the lower frequency predicted data between iterations.

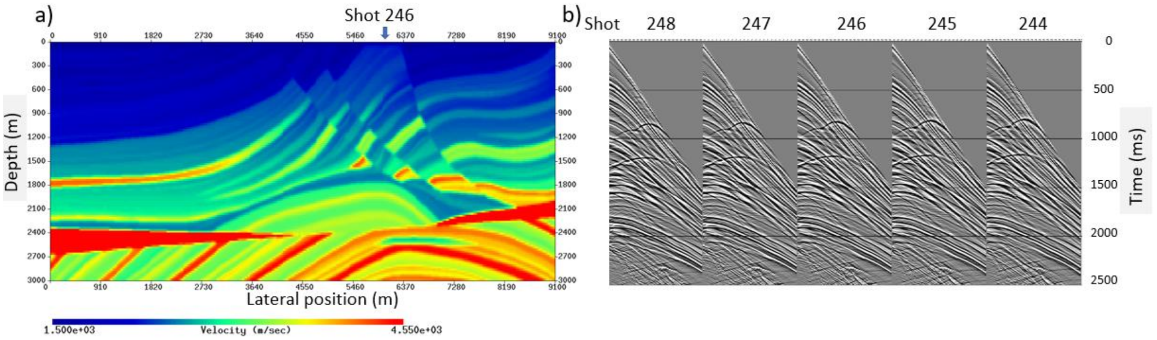

Figure 6 (a) Marmousi model. (b) Synthetic shot records.

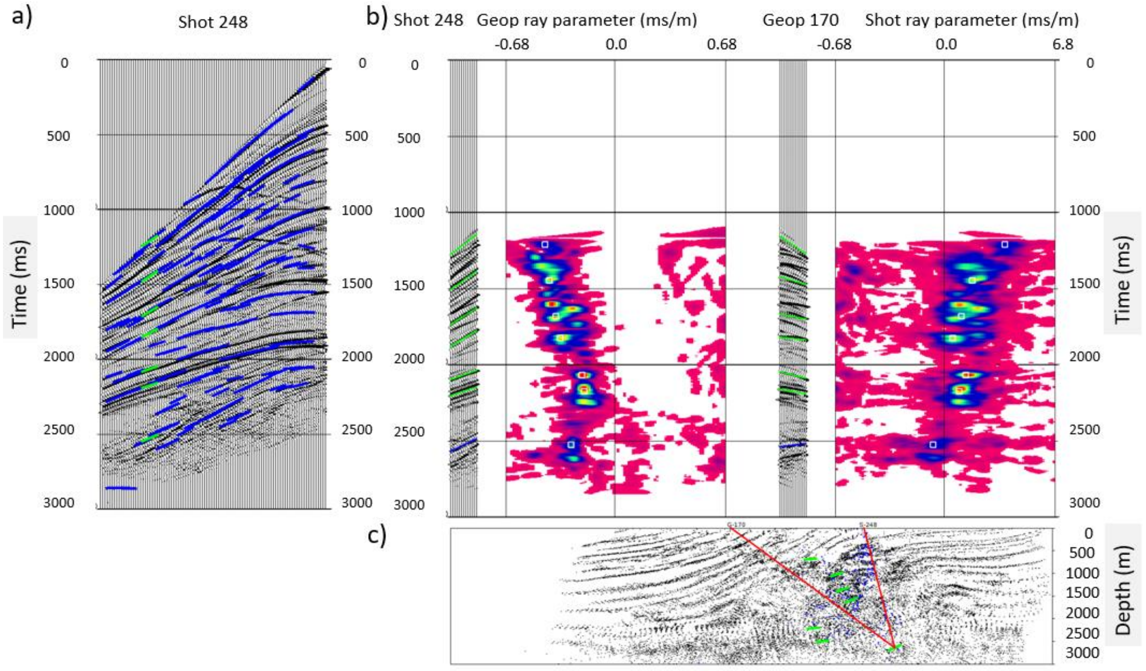

Figure 7 (a) A shot gather with two-way traveltime and geophone ray parameter picks determined by the maximum semblance of the shot and geophone slant stacks. Green lines mark the picks for the active analysis location. (b) Quality control panels for an analysis location, (c) Initial estimates of the scatter positions. Green lines represent scatter positions and dips computed from stereotomography picks at the active analysis location.

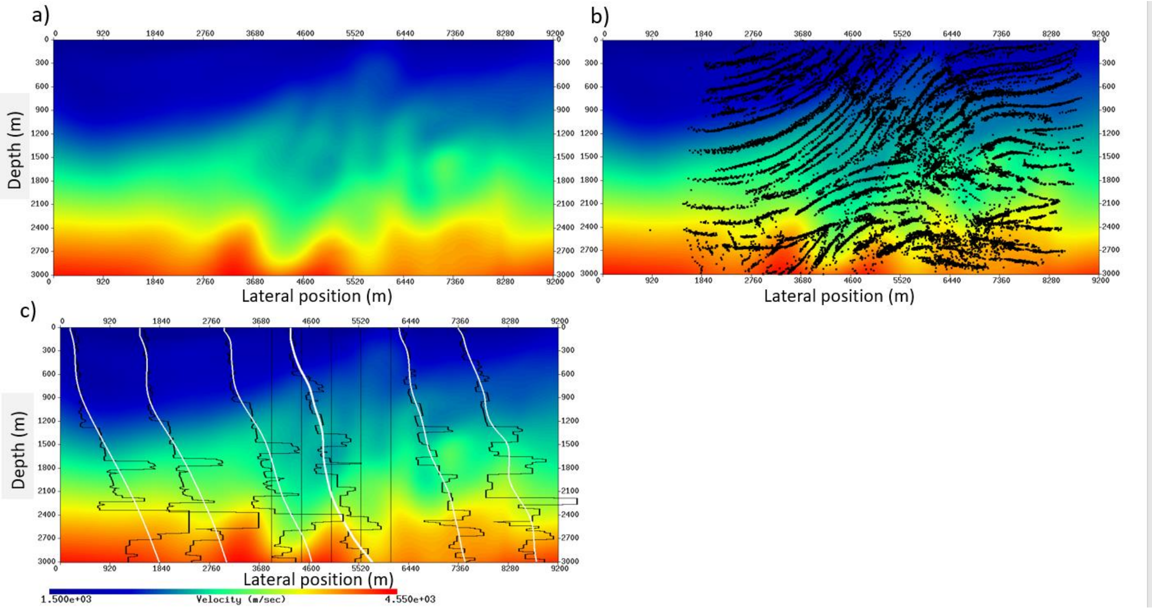

Figure 8 (a) Stereotomography solution of the Marmousi synthetic data set. (b) Scatter positions displayed as black dots. (c) Velocity values at 6 locations are displayed in white for the stereotomography solution and in black for the true model.

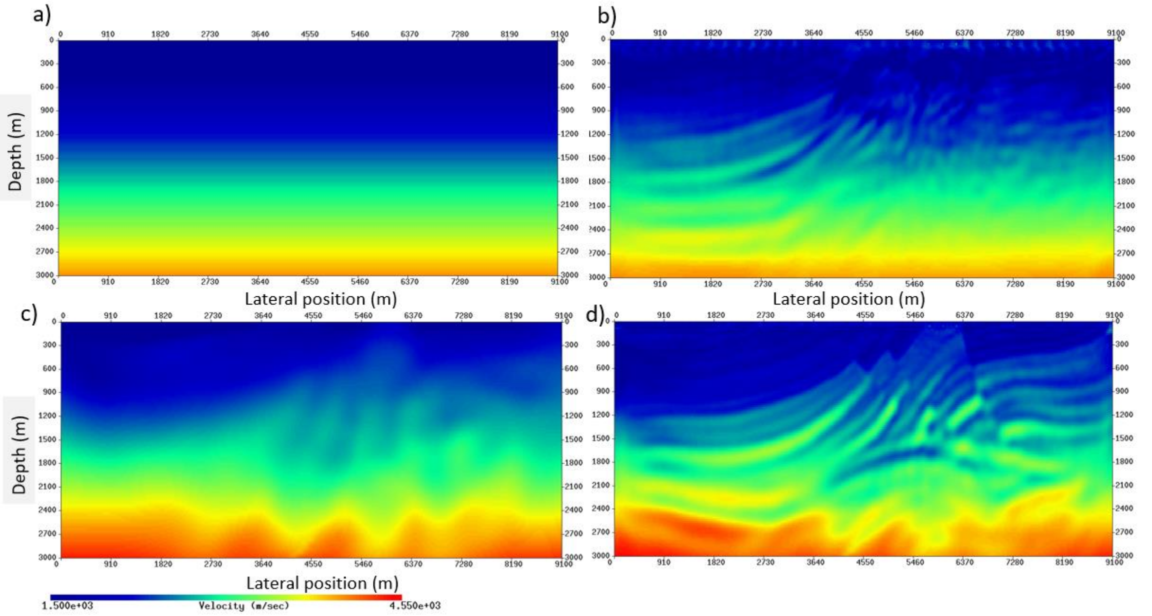

Figure 9 (a) Constant vertical velocity gradient model. (b) FWI solution using (a) as the starting model. (c) Stereotomography solution. (d) FWI solution using (c) as the starting model.

FIELD DATA EXAMPLE

We apply the similar approaches of the wedge model and the Marmousi model in stereotomography to a 2D land dataset. The data used in the example are the vertical component of the dynamite shot records from a 4.5 Km 2D 3C survey acquired at Hussar, Alberta in September 2011. The seismic survey was acquired for a broadband experiment (Margrave et al., 2012). Figure 10a shows the location and the layout of the seismic line and some nearby wells. Figure 10b shows a spherical divergence corrected shot gather, and figure 10c shows the deconvolution and weathering statics correction of the same shot records. To remove the ground roll interference and to improve the lateral coherence, we use Radon transform filter on moveout corrected CDP gathers. Figures 10d shows the same shot records after Radon transform filter in the CDP domain. We use the same approach that we took in the wedge model to automatically pick the refraction arrival time by correlating a CDP stack (Figure 10e) with the moveout corrected and noise attenuated CDP gathers. The moveout correction times are then backed out from the picked reflection arrival times. Figure 10f shows the same shot records with picked reflection arrival times. In order to identify the tie between the well logs and the seismic events, we compare the CDP stack in time with the 8-12-45-55 Hz. synthetic seismograms (Figure 11). In specific, we tie the CDP stack with the Belly Rive, Basal Belly River, Base Fish scales and the Mannville formations. The Belly River reflection is quite noise, we choose to add it for better control on the shallow. We also attempt to do some picking at 200 ms and below 1000 ms.

The reflection arrival times are then used to compute the geophone and shot ray parameters. To remove errors in the reflection arrival times, the geophone and shot ray parameters are repicked using the maximum semblance of the shot and geophone slant stacks (Figure 12a). The final reflection arrival times and ray parameters are then used for stereotomography inversion. The final stereotomography solution is displayed with P-P velocity from well 01-34-025-21W4 and 14-34-025-21W4 (Figure 12b). The velocity values from the stereotomography solution at the well locations agree with the long wavelength trend of the P-P velocity from well logs. Figure 12c shows the scatter position solution. The scatter positions align with Belly River, Basal Belly River, Base Fish Scales and Mannvilles. However, the picks do not cluster as tight as the two synthetic models. This is an indication of some picking error.

To validate the accuracy of the stereotomography solution, we depth migrate the Hussar 2d data set using the stereotomography solution as the velocity model. Figure 13a shows the depth image gathers and figure 13b shows the depth migration result with P-P velocity logs in depth. This result confirms that the stereotomography velocity solution accurately migrates the Hussar 2D data in depth. Further enhancement is possible through residual curvature analysis using the depth image gathers.

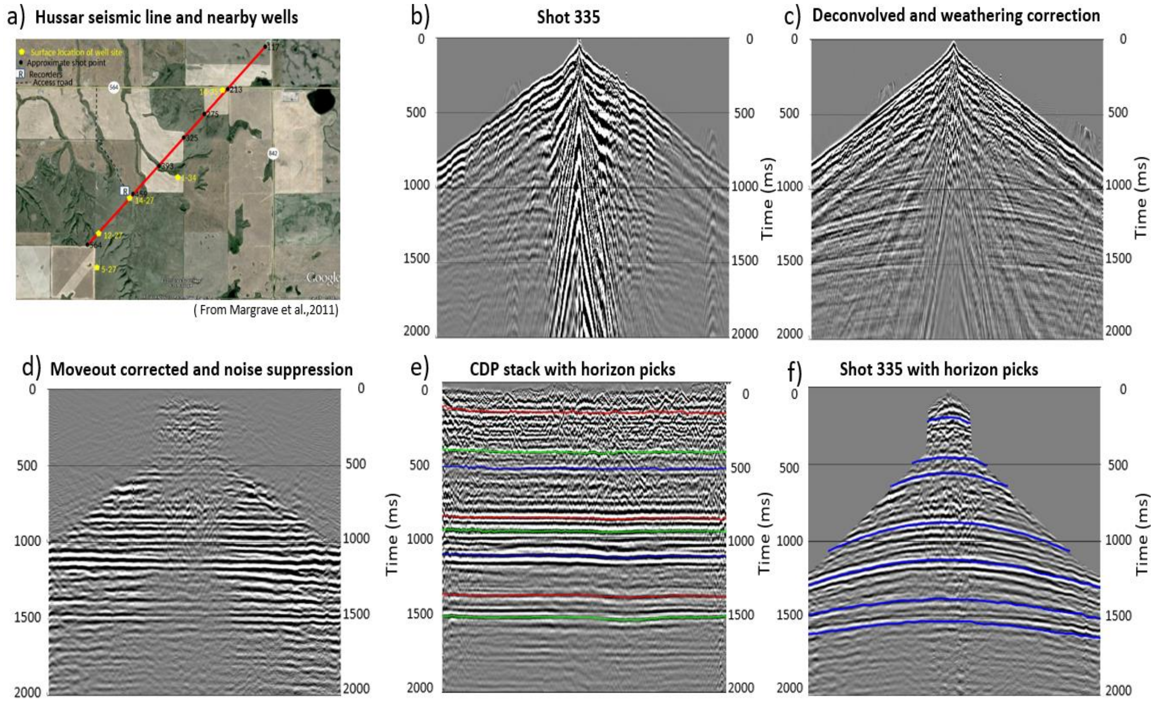

Figure 10 (a) Hussar seismic line and the location of nearby wells. (b) Shot 335 with spherical divergence correction. (c) Shot 335 deconvolved with weathering statics correction. (d) Noise suppression with Radon transform on moveout corrected data. (e) CDP stack with 8 picked horizons. (f) Reflection arrival times picked by correlating (d) and (e).

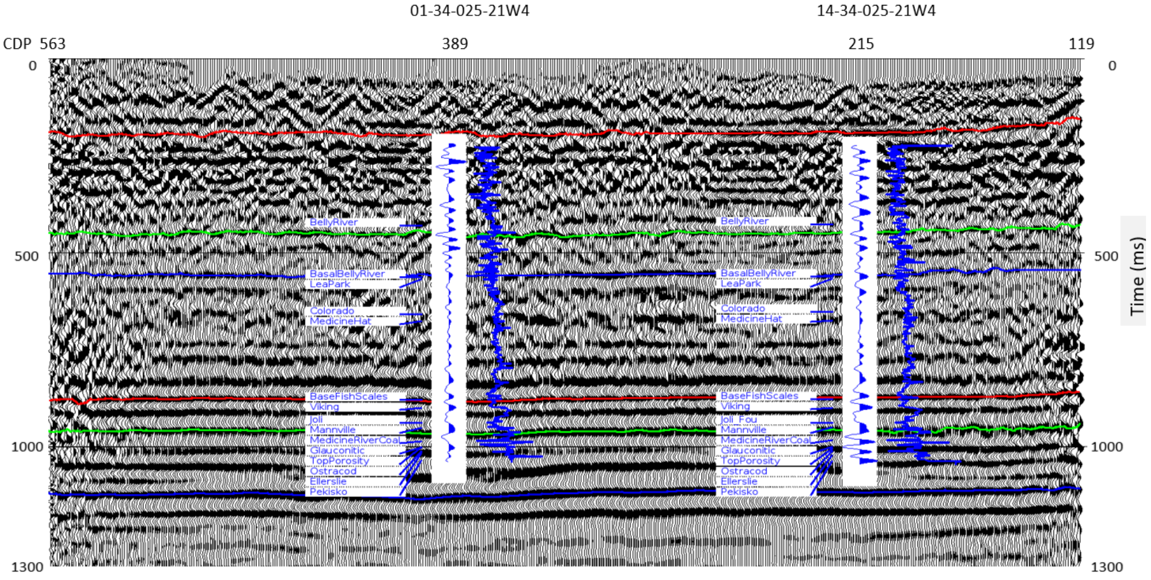

Figure 11. CDP time stack with well ties and synthetic 8-12-45-55 Hz. seismograms to identify reflection events with well tops.

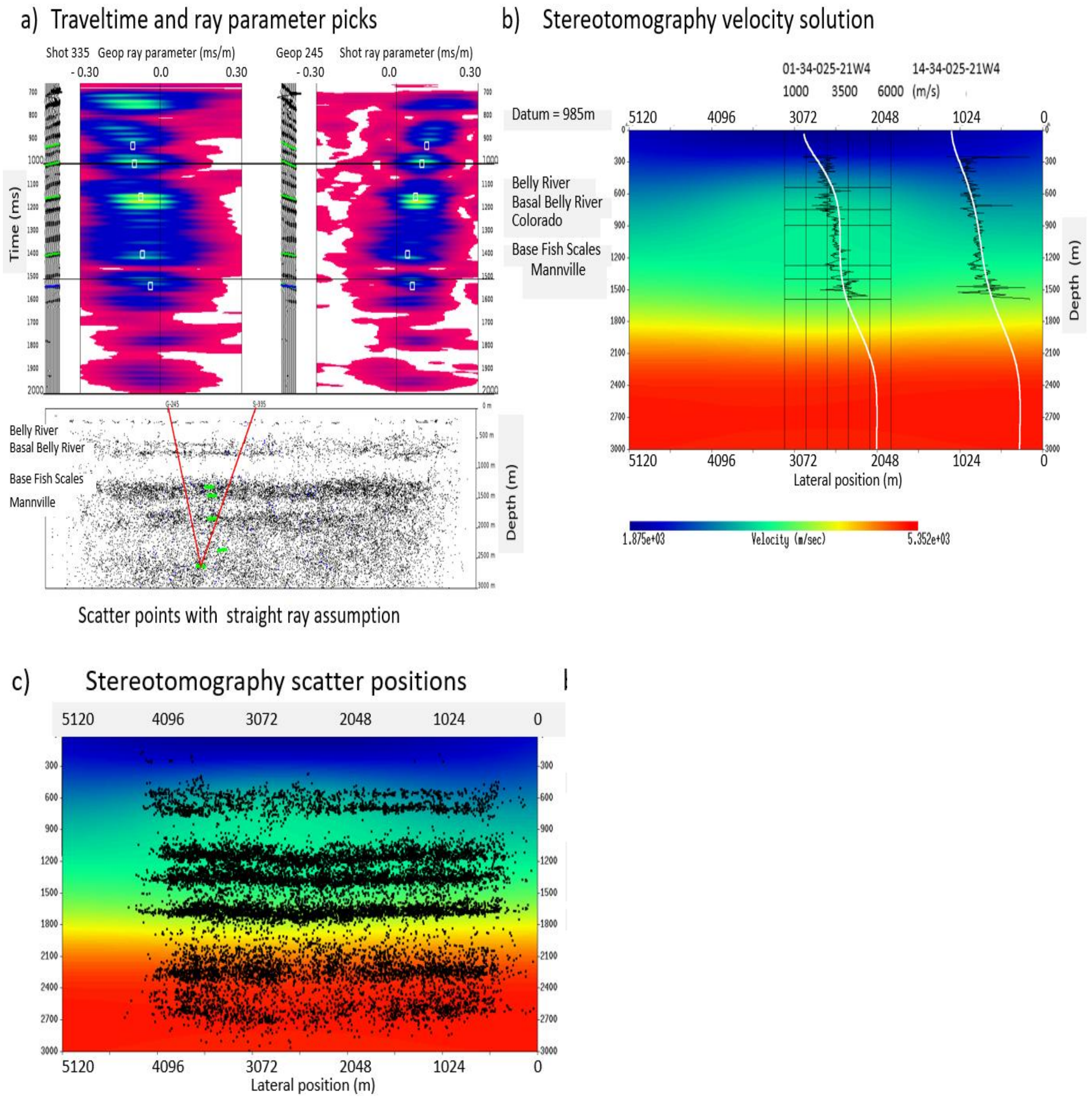

Figure 12 (a) Geophone and shot ray parameters refined by semblance of shot and geophone slant stacks, and scatter point positions computed from all the stereotomography picks using straight-ray and homogeneous velocity assumption. (b) Final stereotomography velocity solution and well ties. Smooth white lines are stereotomography velocity values at well locations. (c) Scatter position solution.

a) Common image gathers

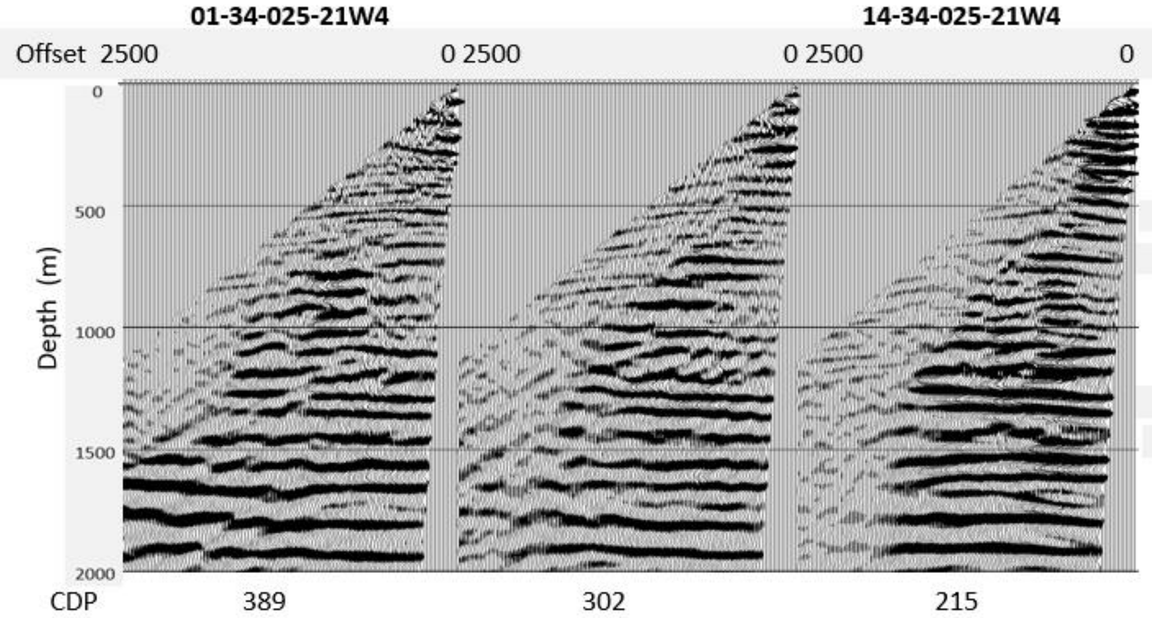

b) Depth migration using stereotomography solution

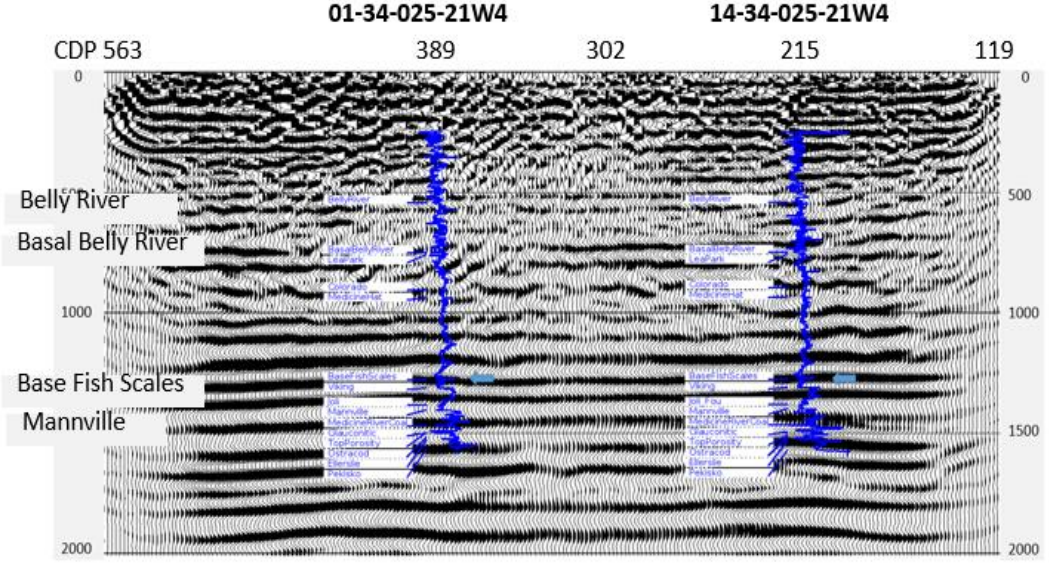

Figure 13 (a) Images gathers at the well locations and one image gather in between the well locations. (b) Depth migration using velocity from stereotomography displayed with P-P velocity logs at well locations 01-34-025-21W4 and 14-34-025-21W4.

.

CONCLUSIONS

We have reviewed the stereotomography method and verified its accuracy and characteristic with a wedge model and the more complex Marmousi model. We showed that the velocity solution from stereotomography does not capture the blocky characteristics of the wedge model, but it resembles velocity gradients centred around the true velocity values. The scatter positions match the velocity boundaries of the wedge model; hence, it is possible to develop a hybrid method that uses the scatter positions to establish the layer boundaries and modify the stereotomography algorithm to estimate a layered based velocity model. The Marmousi model test showed that the solution of stereotomography captured the long wavelength velocity model that helped FWI to converge to a high-resolution model. We noticed that the FWI solution below 2Km was not able to capture the details of the Marmousi model. It is possible that higher order finite-difference propagation in the FWI and adapting the multi-grid FWI approach that shapes the high frequency input to the lower frequency prediction can potentially improve the resolution of FWI solution below 2Km in the Marmousi model. We apply the stereotomography approaches used in the blocky wedge model and the complex Marmousi model to the Hussar 2D dataset. We first track the reflection arrival times on moveout corrected and noise attenuated CDP gathers, and then remove the moveout corrections from the reflection arrival time picks. To correct for the picking errors, shot and geophone ray parameters are repicked automatically using the semblance of the shot and geophone slant stacks. The stereotomography solution was found to be accurately migrating the Hussar 2D data set to a depth section that agrees with the well logs. Further enhancement is possible through residual curvature analysis using the depth image gathers.

ACKNOWLEDGEMENTS

We thank the sponsors of CREWES for continued support. This work was funded by CREWES industrial sponsors, and NSERC (National Science and Engineering Research Council of Canada) through the grantf CRDPJ 461179-13 and CRDPJ 543578-19.

REFERENCES

Bishop, T. N., K. P. Bube, R. T. Langan, P.L. Love, J. R. Resnick, T. T. Shuey, D. A. Spinder, and H.W. Wyld, 1985, Tomographic determination of velocity and depth in laterally varying media: Geophysics, **50**, 903-923.

Billette, F., and G. Lambaré, 1998, Velocity macro-model estimation from seismic reflection data by stereotomography: Geophys. J. Int., 135, 671-690.

Billette, F., S. Le Be´gat, P. Podvin, and G. Lambare´, 2003, Practical aspects and applications of 2D stereotomography: Geophysics, 68, 1008-1021.

Chiu, S. and R. Stewart, 1987, Tomographic determination of three-dimensional seismic velocity structure using well logs, vertical seismic profiles, and surface seismic data: Geophysics, **52**, 1085-1098.

Margrave, G., M. Bertram, K. Hall, K. Innanen, D. Lawton, L. Mewhort, and T. Philips, 2012, A low frequency seismic field experiment: 82nd Annual International Meeting, SEG, Expanded Abstracts, 454-457.

Riabinkin, L.A., 1957, Fundamentals of resolving power of controlled direction reception (CDR) of seismic waves, in Slant Stack Processing, Geophysics Reprint Series, 1919, Soc. Expl. Geophys., Vol. 14. 3-36.

Rieber, F., 1936, A new reflection system with controlled direction sensitity, Geophysics, **1**, 97-106.

Sword C. H., 1987, Tomographic determination of interval velocities from reflection seismic data: The method of controlled directional reception. PhD thesis, Stanford University.

Trad D., 2020, A multigrid approach for time domain FWI: CREWES Research Report, Vol 32.